NJC

ROYAL SOCIETY OF CHEMISTRY

PAPER

View Article Online
View Journal

Cite this: DOI: 10.1039/d1nj01610e

Novel two-dimensional ZnO_2, CdO_2 and HgO_2 monolayers: a first-principles-based prediction†

M. Faraji,[a] A. Bafekry, *[bc] D. Gogova,[d] D. M. Hoat,[ef] M. Ghergherehchi,*[g] N. V. Chuong[h] and S. A. H. Feghhi[b]

Received 2nd April 2021,
Accepted 16th April 2021

DOI: 10.1039/d1nj01610e

rsc.li/njc

In this paper, the existence of monolayers with the chemical formula XO_2, where X = Zn, Cd, and Hg with hexagonal and tetragonal lattice structures is theoretically predicted by means of first principles calculations. Through cohesive energy calculation and phonon dispersion simulation, it has been proven that the two-dimensional XO_2 monolayers proposed are energetically and dynamically stable suggesting their potential experimental realization. Our detailed study demonstrates that these novel newly predicted materials are half-metals and dilute magnetic semiconductors, and they exhibit magnetism in the ground state. The half-metallic character could find many applications in electronic and spintronic devices. Research into the magnetic properties revealed here can enrich theoretical knowledge in this area and provide more potential candidates for XO_2 2D-based materials and van der Waals heterostructures.

1 Introduction

The discovery of the first atomically thin two-dimensional (2D) material, graphene,[1] with magnificent properties that have never been observed before, has triggered tremendous pure scientific and technological interest. A huge number of researchers have devoted enormous efforts to exploration of the monolayer carbon and in the development of novel 2D materials beyond graphene, such as MXenes,[2–6] honeycomb-like Xenes (X = Pb, Sn, Ge, and Si),[6,7] perovskites,[8] and so on. The family of 2D materials has potential applications in nanoscale electronic and optoelectronic devices,[9] and photocatalytic hydrogen productions.[10] Among 2D materials, some behave like insulators,[11] others as semiconductors,[12] metals,[13] semi-metals,[14] half-metals,[15,16] or superconductors.[17] II–VI group semiconductors or group II-chalcogenide materials with the general formula of AX (where A is Zn, Cd or Hg, and X is O, S, Se or Te) have brought many advantages, and they can be utilized in different fields including photovoltaics,[18–20] light-emitting diodes,[21–24] photocatalytic hydrogen production and photoelectrochemical water splitting,[25–27] optical gain,[28–32] CO_2 reduction to CO[33–37] and so on, due to their unique electronic, optical and mechanical properties, and long-term stability. Experimentally, several synthesis methods have been developed for group-II chalcogenide compounds, including the colloidal approach,[38] colloidal ALD,[39] chemical bath deposition,[40] and CVD.[41] Their unique properties have been revealed by a lot of theoretical calculations and analytical methods.[42–47]

Nanoscaled ZnO, CdO, and HgO oxide compounds, have been the subject of many investigations both experimentally and theoretically (based on DFT calculations)[48–52] due to their exceptional physical and chemical properties. In general, they are wide-bandgap semiconductors with potential applications from the ultraviolet to the deep blue spectral region similar to III-nitrides and Ga_2O_3.[53] They have a tendency to be inherent n-type semiconductors and p-type doping poses a serious issue in these materials. In addition to the aforementioned oxide compounds, the transition metal peroxides such as zinc peroxide (ZnO_2), cadmium peroxide (CdO_2), and mercury peroxide (HgO_2) could be new candidates for 2D structures with still unknown properties. The ZnO_2 structure has two oxygen atoms which are linked by a single bond. It has gathered large scientific interest because of the high electronegativity due to the excess of oxygen, especially on a nanoscale level.[54]

Nanostructured ZnO_2 has been successfully utilized in contamination removal from water by UV irradiation[55] as well as in detoxification of mustard gas.[56] ZnO_2 powder is used in many areas, including cosmetics, wear resistance, oral surgeries, and so on.[56] However, while the photocatalytic properties of different 2D

[a] Micro and Nanotechnology Graduate Program, TOBB University of Economics and Technology, Sogutozu Caddesi No. 43 Sogutozu, 06560, Ankara, Turkey
[b] Department of Radiation Application, Shahid Beheshti University, Tehran 1983969411, Iran
[c] Department of Physics, University of Antwerp, Groenenborgerlaan 171, B-2020 Antwerp, Belgium
[d] Department of Physics, University of Oslo, P. O. Box 1048, Blindern, Oslo, Norway
[e] Institute of Theoretical and Applied Research, Duy Tan University, Hanoi 100000, Vietnam
[f] Faculty of Natural Sciences, Duy Tan University, Da Nang 550000, Vietnam
[g] College of Electronic and Electrical Engineering, Sungkyunkwan University, Suwon, Korea
[h] Department of Materials Science and Engineering, Le Quy Don Technical University, Hanoi 100000, Vietnam

† Electronic supplementary information (ESI) available. See DOI: 10.1039/d1nj01610e

metal oxide structures[56–60] have been studied until now, the photocatalytic properties of metal peroxides and related composite materials require detailed investigation. A. G. El-Shamy[61] reported on photocatalytic and tunable photoluminescence performance of carbon quantum dots (CQDs) and ZnO_2 nanocomposites. The results have depicted a larger photocatalytic activity of the CQDs/ZnO_2 nanoparticles than pristine TiO_2, and ZnO_2 structures, against Rh·B, Mo, and MB degradation. CdO_2 is a semiconductor with a bandgap of 2.33 eV. It can be synthesized with different methods[62–64] and utilized in fields such as photocatalysis,[65] as a precursor for CdO n-type semiconductor synthesis,[66] and as an additive material in the rubber and plastic industry.[64] Several theoretical studies (first-principle calculations) have been implemented to understand the CdO_2 structure. For example, A. Zaoui and M. Ferhat[67] reported a thermodynamically and mechanically stable cubic CdO_2 semiconductor structure with a bandgap of 2.9 eV. Nanostructured mercury compounds have been used in different applications.[68–71]

The origin of 1H and 1T phase configuration goes back to MoS_2 different phases, including 1H, 2H, 1T, and so on. Among these phases, two of them are favorable from a structural point of view: 1H-MoS_2 possesses a very rich physics and chemistry. The 1T-MoS_2 structure is a metastable phase, and the most significant distinction between the H and T phase is that the 1T-MoS_2 structure depicts metallic properties, while 1H and 2H is an insulator or a semiconductor.[72] By following the phase structural differences modeling and synthesis, scientists started to develop other structural materials in different phases both theoretically and experimentally, such as semimetal 1H-SnS_2,[73] metallic H-TaS_2,[74] and H-$TaSe_2$,[75] semiconductor 1T-$PtSe_2$,[76] semiconductor 1T-$HfSe_2$,[77] and so on. Obviously, to have different electronic properties of the same materials, it is better to synthesize the material in different phases. XO_2 structures are also following the phase structural differences, which depict different electronic properties behavior. The same as a 1H-MoS_2 monolayer, our 1H-XO_2 structures can be considered as the pristine structures for other XO_2 related structures.

However, there is not a single study on nanostructured HgO_2 in the literature. Theoretically, DFT modeling of HgO_2 can stimulate new research on understanding ructure mercury peroxide compounds. In this paper, the stability as well as structural, electronic and magnetic properties of XO_2 (X = Zn, Cd, Hg) monolayers with hexagonal (1H) and tetragonal (1T) structures have been investigated by means of first-principle calculations. XO_2 monolayers with 1H and 1T structures are found to be dynamically stable. Our calculation results demonstrate that the XO_2 monolayers are half-metal and exhibit magnetism in the ground state, *i.e.* they could open a new door in technology and applications.

2 Method

The structural optimization and electronic properties were performed by the plane-wave basis projector augmented wave (PAW) method in the framework of density-functional theory (DFT). The generalized gradient approximation (GGA) with the Perdew–Burke–Ernzerhof (PBE)[78,79] and hybrid Heyd- Scuseria-Ernzerhof functiona (HSE06)[80] were used for the exchange and correlation contributions as implemented in the Vienna Ab initio Simulation Package (VASP).[81,82] Analysis of the charge transfers in the structures was determined by the Bader technique.[83] The kinetic energy cut-off for plane-wave expansion was set to 500 eV and the energy was minimized until its variation in the following steps became 10^{-8} eV. To get the optimized structures, the total Hellmann–Feynman forces were reduced to 10^{-7} eV $Å^{-1}$. $21 \times 21 \times 1$ Γ centered k-point sampling was used or the primitive unit cells by using Monkhorst–Pack.[84] Monolayers have been modeled with vacuum region 20 Å to avoid interaction between neighboring slabs. The vibrational properties were obtained from the small displacement method as implemented in the PHON code.[85] Simulated scanning tunneling microscopy (STM) images were obtained using the Tersoff–Hamann theory.[86] The STM simulated images were graphically presented using the WSxM software.[87] The training set was prepared by conducting *ab initio* molecular dynamics (AIMD) simulations over $2 \times 2 \times 1$ supercells with $2 \times 2 \times 1$ k-points. AIMD simulations were carried out at 50 and 600 K, each for 1000 time steps. Half of the AIMD trajectories are selected to create the training sets.

3 Monolayer of XO_2 (X = Zn, Cd, Hg)

3.1 Structural properties

The honeycomb structures of the XO_2 monolayers exhibit space group $P3m1$, as shown in Fig. 1(a) and (b), respectively. The hexagonal primitive unit cell is formed by four atoms and the vectors $\vec{a} \neq \vec{b}$ are the translational unit cell vectors. Before gaining insight into the electronic properties, we first calculate

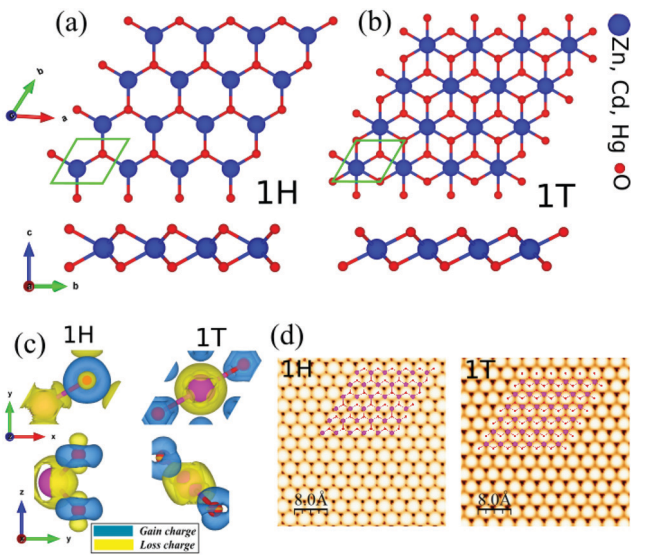

Fig. 1 Atomic structures of XO_2 (X = Zn, Cd, Hg) monolayer (a) -1H and (b) -1T phases, with a primitive unit cell indicated by a green parallelogram. (c) Difference charge density of CdO_2-1H and -1T monolayers. (d) Simulated STM images of CdO_2-1H and -1T monolayers. The inset structure represents repeating the unit cell.

Table 1 The structural, electronic and magnetic parameters of XO_2-1H and -1T monolayers. The corresponding structural, electronic and magnetic parameters including lattice constant a; the bond lengths between X–O atoms $d_{1,2}$; the bond angles between X–O atoms $\theta_{1,2}$; the thickness layer (t); the cohesive energy per atom, (Ecoh); the charge transfer (ΔQ) between atoms; the magnetic moment per unitcell Mtot; and electronic states (ES) are specified as half-metal (HM) and dilute magnetic semiconductor (DMS). The band gap (Eg) of the PBE functional in the up-spin channel

	a (Å)	d_1 (Å)	d_2 (Å)	t (Å)	$\theta_{1,2}$ (°)	E_{coh} (Å)	ΔQ (eV per atom)	Φ (e)	ES (eV)	M_{tot} (μ_B)	E_g (eV)
ZnO_2-1H	3.08	2.07	2.11	2.57	96.21, 61.47	2.88	1.33	7.72	HM	2	0
ZnO_2-1T	3.11	2.03	2.60	2.57	79.84, 100.13	3.00	1.40	7.46	DMS	2	0.25
CdO_2-1H	3.44	2.27	2.20	2.57	98.44, 58.05	2.55	1.27	7.26	HM	2	0
CdO_2-1T	3.40	2.23	2.82	2.57	100.138, 78.67	2.62	1.32	7.24	DMS	2	0.05
HgO_2-1T	3.00	2.24	2.89	2.57	80.21, 99.80	2.03	1.22	7.21	DMS	2	0.21

the geometrical structure, with full optimization of all the atoms and determine the crystal lattice parameters. The calculated lattice constants of the ZnO_2 are equal to 3.08 Å (1H) and 3.11 Å (1T), while the bond lengths d_1 and d_2 are determined to be 2.07 Å (1H) and 2.11 Å (1T), respectively. The two angles of the Zn–O–Zn bonds in the ZnO_2-1H (1T) lattice are 96.21° (79.84°) and 61.47° (100.13°), *i.e.* slightly deviating from 120° and indicating the in-plane anisotropy of the lattice. In the CdO_2-1H (-1T), we found that the lattice parameters increase to 3.44 (3.40) Å, while the bond lengths are d_1 = 2.27 (2.23) Å and d_2 = 2.20 (2.82) Å (Table 1). In addition, the bond angles are the same θ_1 = 98.44° and θ_2 = 58.05° for each CdO_2-1H layer, and the thickness of CdO_2 is determined to be 2.55 Å. Notice that in the case of a HgO_2-1T structure, the lattice parameter is determined to be 3.00 Å. We found out that the bond lengths are 2.24 and 2.89 Å, while the bond angles are calculated to be 80.21 and 99.80°, respectively. The difference charge density of CdO_2-1H and -1T is depicted in Fig. 1(c), where the blue and yellow regions represent the charge accumulation and depletion, correspondingly. The difference charge density ($\Delta\rho$) is defined as follows:

$$\Delta\rho = \rho_{XO2} - \rho_X - \rho_O \quad (1)$$

where ρ_{XO2}, ρ_X and ρ_O represents the charge densities of the XO_2 and isolated atoms, respectively. From the difference charge density, we found out that the negatively charged O atoms are surrounded by positively charged X atoms. We discover that each O atom gains about 1.33 e, and 1.27 e from the adjacent Zn and Cd atoms in ZnO_2-1H and CdO_2-1H structures, respectively. Meanwhile, in the 1T structure of ZnO_2, CdO_2 and HgO_2, each O atom gains about 1.40, 1.32 and 1.22 e from the adjacent Zn, Cd and Hg atoms. The charge redistribution is due to the different electronegativity of Zn (1.65), Cd (1.69), Hg (2.00) and O (3.44). The simulated STM image of the CdO_2-1H (left) and -1T (right) is illustrated in Fig. 1(d), which overlayed with its structure. From the theoretically predicted STM images, it is easy to recognize and correlate them with the corresponding atomistic structure. One can see that the the O atoms are brighter than the Cd ones. Cohesive energy, which is defined as the energy required to separate condensed material into isolated free atoms, is one of the most important physical parameters for quantifying the energetic stability of materials. The cohesive energy per atom was calculated using the following equation:

$$E_{coh} = \frac{E_{tot} - E_X - 2E_O}{n_{tot}} \quad (2)$$

where E_X and E_{Bi} represent the energies of isolated single X (Zn, Cd and Hg) and O atoms, n_{tot} is the total number of unit cells, respectively; E_{tot} represents the total energy of the XO_2 monolayer. The cohesive energies of ZnO_2-1H and -1T, are found to be −2.88 and −3.00 eV per atom, respectively, which indicates that the formation of 1T is more favorable than 1H. In addition, the calculated cohesive energy of CdO_2-1H (−2.55 eV per atom) and CdO_2-1T (−2.62 eV per atom) indicates that the magnetic ground state of the 1T is more favorable. Notice that the cohesive energy of HgO_2-1T is obtained as −2.03 eV per atom. The more negative values for cohesive energies suggest that the energetically more stable monolayer, and the structures represent more stability when the atoms get lighter.

Now we examine the dynamical and thermal stability of the XO_2 monolayer by evaluating the phonon dispersion relation and AIMD trajectories at 500 K, respectively. The dynamical stability is verified by calculating the phonon band dispersions, as presented in Fig. 2(a–f). Apparently, phonon branches are free from any imaginary frequencies indicating the dynamical stability of all the XO_2 monolayers, except HgO_2-1H, as depicted

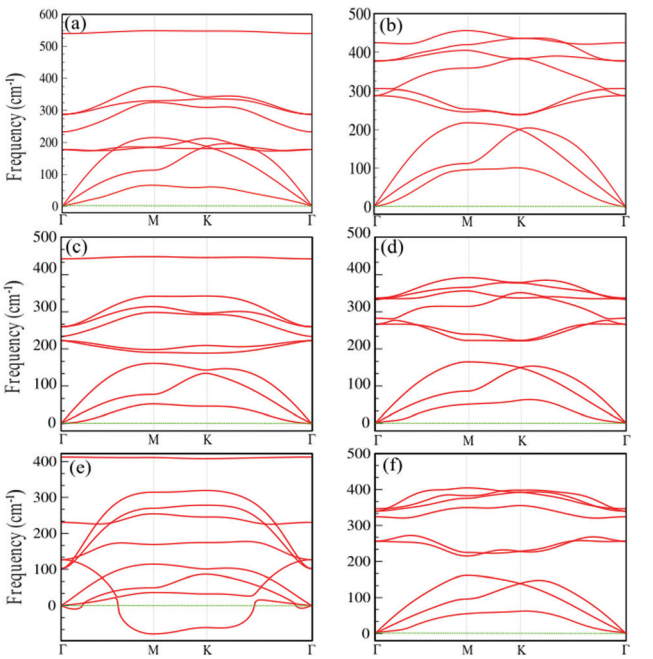

Fig. 2 Phonon band dispersion of (a) ZnO_2-1H, (b) ZnO_2-1T, (c) CdO_2-1H, (d) CdO_2-1T and (e) HgO_2-1H and (f) HgO_2-1T monolayers.

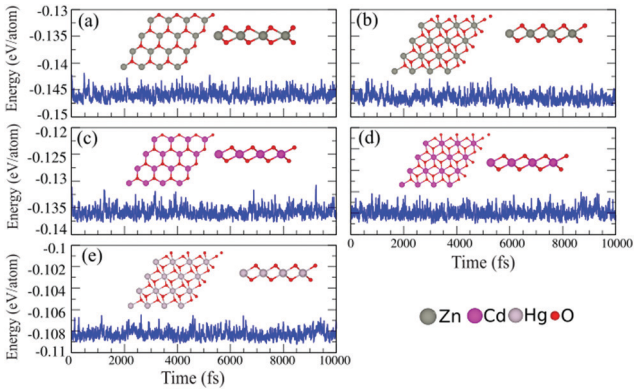

Fig. 3 *Ab initio* molecular dynamics (AIMD) for the (a) ZnO_2-1H, (b) ZnO_2-1T, (c) CdO_2-1H, (d) CdO_2-1T and (e) HgO_2-1T monolayers at room temperature. The top and side views of the structures after 5 ps of simulation indicated as the inset.

in Fig. 2(e). This demonstrates the instability of the HgO_2-1H monolayer. *Ab initio* molecular dynamics (AIMD) for the studied monolayers at room temperature is shown in Fig. 3(a–e). The top and side views of the structures after 5 ps of simulation as insets are shown in Fig. 3. Analysis of the AIMD trajectories also shows that the structure could stay intact at 300 K, with very stable energy and temperature profiles, proving the thermal stability of the XO_2 monolayer.

3.2 Electronic and magnetic properties

The electronic band structure of the XO_2 monolayers are depicted in Fig. 4(a–e). The contour plots of the electron localization function (ELF) are shown in the top of the panels, where red and blue color indicate high and low electron density, respectively. Notice that ZnO_2-1H exhibits a half-metallic behavior with valence bands in the ↓ spin channel, crossing the Fermi level and has 2 μ_B magnetic moment. Meanwhile, ZnO_2-1T shows semiconducting characteristics in both the ↑ and ↓ spin channels, *i.e.*, it is dilute. The direct band gap of ZnO_2-1T in the ↓ spin channels is calculated to be 0.21 eV, while the valence band minimum (VBM) and conduction band maximum (CBM) are located along the K–Γ points. Notice that, we can see a direct band gap with a value of 0.27 meV, which is located along the Γ–M points. The magnetic moment of the ZnO_2-1T is determined to be 2 μB in the ground state. Similarly ZnO_2 and CdO_2 exhibit HM and DMS in the 1H and 1T phase structures and our results show that the magnetic moment of the CdO_2-1T and -1H is 2 μB in the ground state. In the ↓ spin channels of the CdO_2-1T, we can see a narrow direct band gap of 50 meV, while the VBM and CBM are located between the K and Γ points. Paying attention, we found a narrow direct band gap with a value of 110 meV, which is located between the Γ and M points. In the case of HgO_2-1T, the ↑ and ↓ spin channels are split, resulting in a DMS and inducing 2 μB magnetic moment in the ground state. The indirect band gap of the HgO_2-1T in the ↓ spin channels is calculated to be 0.25 eV, while the VBM and CBM are located along the Γ–M points. Notice that a direct band gap of 0.35 eV is shown along the K–Γ points.

It should be noted that bulk trigonal and cubic ZnO_2 structures have depicted magnetic and non-magnetic properties, respectively. A trigonal ZnO_2 structure has a band gap of about 4 eV with insulating properties, while a cubic ZnO_2 structure depicts a semiconductor with a band gap of 2.157 eV. For the bulk CdO_2, both cubic and monoclinic structures have depicted non-magnetic properties. Both CdO_2 structures are an indirect semiconductor with a bandgap of 1.268 and 2.36 eV for cubic and monoclinic structures, respectively. Finally, for the bulk HgO_2 with orthorhombic and monoclinic structures, both have been depicted as non-magnetic materials, with an indirect bandgap of 0.308 and 0.212 eV, respectively.

Since these monolayers are semiconductors in the ↑ and ↓ spin channels, the HSE06 functional was also used to study the electronic band structures, shown in Fig. S2 (ESI†). Based on the acquired band structure by the HSE06 method, the ZnO_2-1H and ZnO_2-1T monolayers exhibit a half-metallic characteristic. Our results shows that CdO_2 shows DMS and half-metallic behaviors in the 1H and 1T phase structures, respectively. In the case of HgO_2-1T, the ↑ (↓) spin channels are a semiconductor (metal), resulting in half-metallicity in the ground state.

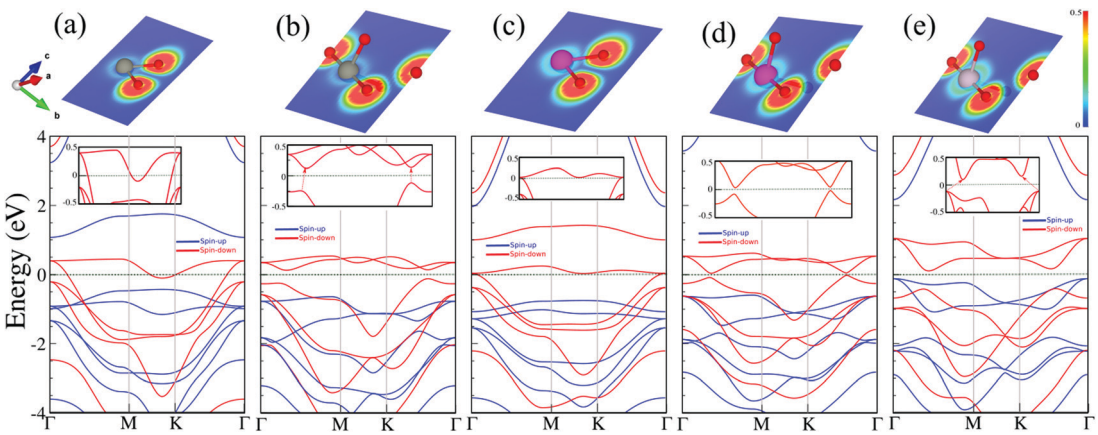

Fig. 4 Electronic band structure of (a) ZnO_2-1H, (b) ZnO_2-1T, (c) CdO_2-1H, (d) CdO_2-1T and (e) HgO_2-1T. Contour plots of the electron localization function (ELF) are shown in the top of the panels. Red (blue) color indicates high (low) electron density. The zero of energy is set to the Fermi-level.

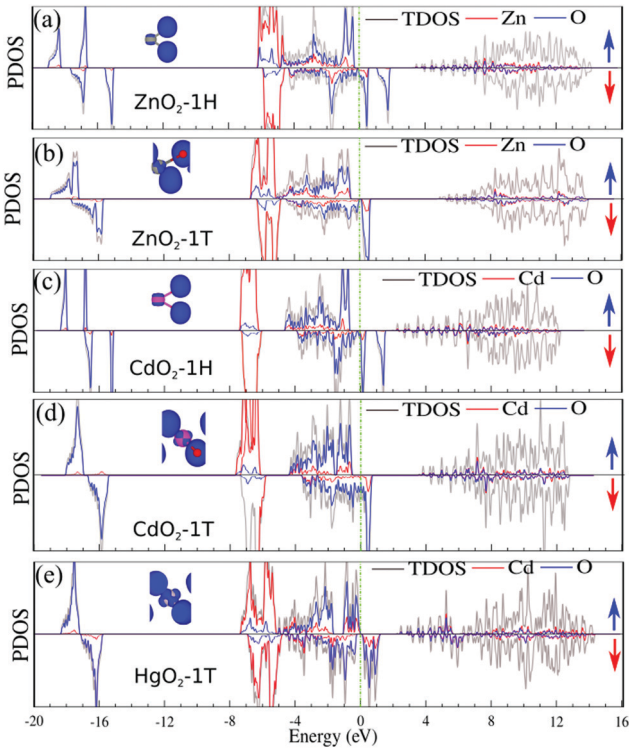

Fig. 5 DOS and PDOS of (a) ZnO_2-1H, (b) ZnO_2-1T, (c) CdO_2-1H, (d) CdO_2-1T and (e) HgO_2-1T. Difference spin density is shown in the insets. The blue and yellow regions represent the ↑ and ↓ spin states, respectively. The zero of energy is set to the Fermi-level.

In order to explain the origin of the electronic states, the density of states (DOS) and projected DOS (PDOS) are shown in Fig. 5. The contribution of different atomic orbitals is indicated in Fig. S1 in the ESI.† Evidently, the metallic character of the ZnO_2-1H and CdO_2–H comes from the O atoms in the ↓ spin channel, while Zn and Cd atoms do not show any contribution (see Fig. 5). From DOS and PDOS of the ZnO_2-1T and CdO_2-T, we can see that the VBM originates from the O-$p_{x,y}$ orbitals (↑ spin channels), while the CBM consists of O-p_z orbital states (↓ spin channels). Unlike the ZnO_2-1T, we found that the VBM and CBM of HgO_2-1T originates from the O-p_z (↑ spin channel). The difference spin density is calculated from the difference spin density between ↑ and ↓ spin channels. In order to analyse the magnetism, the difference spin density of the XO_2 is illustrated in the inset of Fig. 5. One can conclude that the magnetism mainly originates from the O atoms in XO_2.

Due to the weak screening of the Coulomb interaction in 2DM, it is expected that the Hubbard U will be larger than in three-dimensional materials, and thus the energy band gap may be expected to be enhanced significantly. We investigate effects of correlation by varying the value of the Hubbard U, since the accurate value of U has not been determined for ZnO_2-1H and CdO_2–H monolayers. The electronic band structure of ZnO_2-1H and CdO_2–H monolayers as a function of Hubbard U, is shown in Fig. S3(a and b) (ESI†). We see from Fig. S3(a) (ESI†) that the ZnO_2-1H still maintains the DHM feature even when considering the effect of the Hubbard U. With increase of Hubbard U, the 3d orbitals of the Zn atom states do not change near the Fermi-level, indicating the robustness of the energy bands against the correlation effect in Zn-3d electrons. The correlation effects on the electronic properties of CdO_2–H are significant and we can see that the CdO_2–H still maintains the DMS character. Notice, that the band gap increasing in the ↓ spin channel is a result of a cooperative effect of electron correlation for the CdO_2–H. Our results show that the band gap (↓ spin channel) of CdO_2–H increases from 1.25 eV for U = 1 eV to 2 eV for U = 8 eV, and therefore DMS remains for U = 1–8 eV.

4 Conclusions

In summary, we have investigated the structural, dynamical stability, thermal stability, electronic and magnetic properties of novel 2D materials XO_2 (X = Zn, Cd, Hg) – by using first-principles calculations. Our computational results have proven the energetic and dynamic stability of this new class of 2D materials with amazing properties. Thus, our study could trigger the search for methods of synthesis of ZnO_2, CdO_2 and HgO_2 monolayers and exploration of their high application potential. Research into the magnetic properties revealed here can enrich theoretical knowledge in this area and provide more potential candidates for XO_2 2D-based materials and van der Waals heterostructures.

Data availability

The data that support the findings of this study are available from the corresponding author upon request.

Conflicts of interest

The authors declare that they have no known competing financial interests or personal relationships that could have appeared to influence the work reported in this paper.

Acknowledgements

This work was supported by the National Research Foundation of Korea (NRF) grant funded by the Korea Government (MSIT) (NRF-2015M2B2A4033123).

References

1 K. S. Novoselov, A. K. Geim, S. V. Morozov, D. Jiang, Y. Zhang, S. V. Dubonos, I. V. Grigorieva and A. A. Firsov, *Science*, 2004, **306**(5696), 666–669.
2 A. Bafekry, B. Akgenc, M. Ghergherehchi and F. M. Peeters, *J. Phys.: Condens. Matter*, 2020, **29**, 355504.
3 A. Bafekry, C. V. Nguyen, C. Stampfl, B. Akgenc and M. Ghergherehchi, *Phys. Status Solidi B*, 2020, **257**(12), 2000343.
4 E. M. D. Siriwardane, I. Demiroglu, C. Sevik, F. M. Peeters and D. Cakir, *J. Phys. Chem. C*, 2020, **124**(39), 21293–21304.

5 Q. Zhao, M. Seredych, E. Precetti, C. E. Shuck, M. Harhay, R. Pang, C. Shan and Y. Gogotsi, *ACS Nano*, 2020, **14**(9), 11787–11798.
6 A. Bafekry, F. Shojaei, M. M. Obeid, M. Ghergherehchi, C. Nguyen and M. Oskouian, *RSC Adv.*, 2020, **10**, 31894.
7 A. Bafekry, F. Shojai, D. M. Hoat, M. Ghergherehchi, C. Nguyen and M. Shahrokhi, *RSC Adv.*, 2020, **10**, 30398.
8 Y. Chen, Y. Sun, J. Peng, J. Tang, K. Zheng and Z. Liang, *Adv. Mater.*, 2017, 1703487.
9 S. Kang, D. Lee, J. Kim, A. Capasso, C. H. Lee, G. H. Lee, H. S. Kang and J. W. Park, *2D Mater.*, 2020, **7**(2), 022003.
10 Q. Su, Y. Li, R. Hu, F. Song, S. Liu, C. Guo, S. Zhu, W. Liu and J. Pan, *Adv. Sustainable Syst.*, 2020, 2000130.
11 J. Yin, J. Li, Y. Hang, J. Yu, G. Tai, X. Li, Z. Zhang and W. Guo, *Small*, 2016, **12**(22), 2942–2968.
12 M. Khosravi, G. Moafpouriana and H. A. Badehianb, *Optik*, 2020, **218**, 165247.
13 D. Zhou, Q. Meng, N. Si, X. Zhou, S. Zhai, Q. Tang, Q. Ji, M. Zhou, T. Niu and H. Fuchs, *ACS Nano*, 2020, **14**, 2385–2394.
14 H. Yang, M. Schmidt, V. Suss, M. Chan, F. F. Balakirev, R. D. McDonald, S. S. P. Parkin, C. Felser, B. Yan and P. J. W. Moll, *New J. Phys.*, 2018, **20**, 043008.
15 A. Bafekry, B. Mortazavic and S. Farjami Shayesteha, *J. Magn. Magn. Mater.*, 2019, **491**, 165565.
16 A. Bafekry, C. Stampfl and M. P. Francois, *Sci. Rep.*, 2020, **10**, 213.
17 V. Kamysbayev, A. S. Filatov, H. Hu, X. Rui, F. Lagunas, D. Wang, R. F. Klie and D. V. Talapin, *Science*, 2020, **369**(6506), 979–983.
18 R. W. Crisp, F. S. M. Hashemi, J. Alkemade, N. Kirkwood, G. Grimaldi, S. Kinge, L. D. A. Siebbeles, J. R. V. Ommen and A. J. Houtepen, *Adv. Mater. Interfaces*, 2020, 1901600.
19 D. B. Li, S. S. Bista, Z. Song, R. A. Awni, K. K. Subedi, N. Shrestha, P. Pradhan, L. Chen, E. Bastola, C. R. Grice, A. B. Phillips, M. J. Heben, R. J. Ellingson and Y. Yan, *Nano Energy*, 2020, **73**, 104835.
20 P. Labouchere, A. K. Chandiran, T. Moehl, H. Harms, S. Chavhan, R. Tena-Zaera, M. K. Nazeeruddin, M. Graetzel and N. Tetreault, *Adv. Energy Mater.*, 2014, 1400217.
21 J. Lim, Y. S. Park, K. Wu, H. J. Yun and V. I. Klimov, *Nano Lett.*, 2018, **18**(10), 6645–6653.
22 J. Lim, B. G. Jeong, M. Park, J. K. Kim, J. M. Pietryga, Y. S. Park, V. I. Klimov, C. Lee, D. C. Lee and W. Ki Bae, *Adv. Mater.*, 2014, **26**, 8034–8040.
23 J. Roh, Y. S. Park, J. Lim and V. I. Klimov, *Nat. Commun.*, 2020, **11**, 271.
24 Y. Altintas, B. Liu, P. L. Hernandez-Martinez, N. Gheshlaghi, F. Shabani, M. Sharma, L. Wang, H. Sun, E. Mutlugun and H. V. Demir, *Chem. Mater.*, 2020, **32**(18), 7874–7883.
25 C. T. Altaf, M. Faraji, A. Kumtepe, N. Abdullayeva, N. Yilmaz, E. Karagoz, A. Bozbey, H. Kurt, M. Sankir and N. D. Sankir, *J. Alloys Compd.*, 2020, **828**, 154472.
26 M. M. Obeid, C. Stampfl, A. Bafekry, Z. Guane, H. R. Jappor, C. V. Nguyen, M. Naseri, D. M. Hoat, N. N. Hieu, A. E. Krauklis, T. V. Vu and D. Gogova, *Phys. Chem. Chem. Phys.*, 2020, **22**, 15354–15364.
27 M. M. Obeida, A. Bafekry, S. U. Rehmand and C. V. Nguyenf, *Appl. Surf. Sci.*, 2020, **534**, 147607.
28 O. Erdem, S. Foroutan, N. Gheshlaghi, B. Guzelturk, Y. Altintas and H. V. Demir, *Nano Lett.*, 2020, **20**(9), 6459–6465.
29 B. T. Diroll, D. V. Talapin and R. D. Schaller, *ACS Photonics*, 2017, **4**(3), 576–583.
30 V. Pinchetti, F. Meinardi, A. Camellini, G. Sirigu, S. Christodoulou, W. K. Bae, F. D. Donato, L. Manna, M. Zavelani-Rossi, I. Moreels, V. I. Klimov and S. Brovelli, Effect of Core/Shell Interface on Carrier Dynamics and Optical Gain Properties of Dual-Color Emitting CdSe/CdS Nanocrystals, *ACS Nano*, 2016, **10**(7), 6877–6887.
31 J. Lim, Y. S. Park and V. I. Klimov, Optical gain in colloidal quantum dots achieved with direct-current electrical pumping, *Nat. Mater.*, 2018, **17**, 42–49.
32 K. Wu, Y. S. Park, J. Lim and V. I. Klimov, *Nat. Mater.*, 2018, **17**, 42–49.
33 F. Zhang, Y. H. Li, M. Y. Qi, Z. R. Tang and Y. J. Xu, *Appl. Catal., B*, 2020, **268**, 118380.
34 D. Tan, W. Lee, Y. E. Kim, Y. N. Ko, Y. E. Jeon, J. Hong, S. K. Jeong and K. T. Park, *ACS Sustainable Chem. Eng.*, 2020, **8**(29), 10639–10645.
35 N. Q. Thang, A. Sabbah, L. C. Chen, K. H. Chen, L. V. H. C. M. Thi and P. V. Viet, *Chem. Eng. Sci.*, 2021, **229**, 116049.
36 F. Y. Gao, R. C. Bao, M. R. Gaoa and S. H. Yu, *J. Mater. Chem. A*, 2020, **8**, 15458–15478.
37 P. Prabhu, V. Jose and J. M. Lee, *Adv. Funct. Mater.*, 2020, 1910768.
38 M. J. Grotevent, C. U. Hail, S. Yakunin, D. Bachmann, M. Calame, D. Poulikakos, M. V. Kovalenko and I. Shorubalko, *Adv. Sci.*, 2021, **8**, 2003360.
39 L. Piveteau, D. N. Dirin, C. P. Gordon, B. J. Walder, T. C. Ong, L. Emsley, C. Coperet and M. V. Kovalenko, *Nano Lett.*, 2020, **20**(5), 3003–3018.
40 R. Vignesh, B. A. kumar, A. Muthuvinayagam, T. Elangovan, K. Kaviyarasu, G. Theophil Anand and G. Ramalingam, *Mater. Today: Proc.*, 2020, 2214–7853.
41 J. Luo, Z. Zheng, S. Yan, M. Morgan, X. Zu, X. Xiang and W. Zhou, *ACS Photonics*, 2020, **7**(6), 1461–1467.
42 N. Gheshlaghi, M. Faraji and H. Sedaghat Pisheh, Structural dependent, dielectric and conduction analysis of CdSe based quantum dots, *Appl. Sci.*, 2019, 401.
43 N. Gheshlaghi, M. Faraji and H. Sedaghat Pisheh, *SN Appl. Sci.*, 2020, **2**, 745.
44 N. Gheshlaghi, H. Sedaghat Pisheh and H. Unlu, *Superlattices Microstruct.*, 2017, **111**, 156–165.
45 N. Gheshlaghi, H. Sedaghat Pisheh, M. R. Karim and H. Unlü, *Energy Procedia*, 2016, **102**, 152–163.
46 N. Gheshlaghi, H. Sedaghat Pisheh, M. R. Karim, D. Malkoc and H. Unlu, *Superlattices Microstruct.*, 2016, **111**, 486–494.
47 H. Sedaghat Pisheh, N. Gheshlaghi and H. Unlu, *Physica E*, 2017, **85**, 334–339.
48 R. Chandiramouli and B. G. Jeyaprakash, *Solid State Sci.*, 2013, **16**, 102–110.
49 A. Schleife, F. Fuchs, J. Furthmuller and F. Bechstedt, *Phys. Rev. B: Condens. Matter Mater. Phys.*, 2006, **73**, 245212.

50 S. Vyas, *Johnson Matthey Technol. Rev.*, 2020, **64**(2), 202–218.
51 K. Harun, N. A. Salleh, B. Deghfel, M. K. Yaakob and A. A. Mohamad, *Results Phys.*, 2020, **16**, 102829.
52 P. A. Glans, T. Learmonth, K. E. Smith, J. Guo, A. Walsh, G. W. Watson, F. Terzi and R. G. Egdell, *Phys. Rev. B: Condens. Matter Mater. Phys.*, 2005, **71**(23), 235109.
53 D. Gogova, A. Kasic, H. Larsson, B. Pecz, R. Yakimova, B. Magnusson, B. Monemar, F. Tuomisto, K. Saarinen, C. Miskys, M. Stutzmann, C. Bundesmann and M. Schubert, *J. Appl. Phys.*, 2004, **43**(4A), 1264–1268.
54 D. A. Zatsepin, D. W. Boukhvalov, A. F. Zatsepin, Y. A. Kuznetsova, D. Gogova, V. Y. Shur and A. A. Esin, *Superlattices Microstruct.*, 2018, **120**, 90–100.
55 D. Yanga, M. A. Gondalb, Z. H. Yamanib, U. Baigb, X. Qiaoc, G. Liua, Q. Xud, D. Xiange, J. Maof and K. Shena, *Mater. Sci. Semicond. Process.*, 2017, **57**, 124–131.
56 D. A. Giannakoudakis, M. Florent, R. Wallace, J. Secor, C. Pkarwacki and T. J. Bandosz, *Appl. Catal., B*, 2018, **226**, 429–440.
57 R. Saravanan, M. Mansoob Khan, V. K. Gupta, E. Mosquera, F. Gracia, V. Narayanan and G. A. Stephen, *J. Colloid Interface Sci.*, 2015, **425**(15), 126–133.
58 R. Saravanan, H. Shankar, T. Prakash, V. Narayanan and A. Stephen, *Mater. Chem. Phys.*, 2011, **125**, 277–280.
59 T. Munawar, S. Yasmeen, F. Hussain, K. Mahmood, A. Hussain, M. Asghar and F. Iqbal, *Mater. Chem. Phys.*, 2020, **249**, 122983.
60 E. A. Abdelrahman and R. M. Hegazey, Facile Synthesis of HgO Nanoparticles Using Hydrothermal Method for Efficient Photocatalytic Degradation of Crystal Violet Dye Under UV and Sunlight Irradiation, *J. Inorg. Organomet. Polym. Mater.*, 2019, **29**, 346–358.
61 A. g. El-Shamy, *Synth. Met.*, 2020, **267**, 116472.
62 X. Han, R. Liu, Z. Xu, W. Chen and Y. Zheng, *Electrochem. Commun.*, 2005, **7**, 1195–1198.
63 L. Beigi and V. Saheb, *Nano-Struct. Nano-Objects*, 2017, **9**, 13–18.
64 Y. Liu, Y. C. Zhang and M. Zhang, *Mater. Lett.*, 2010, **64**, 1779–1781.
65 Y. Liu, Y. C. Zhang and X. F. Xu, *J. Hazard. Mater.*, 2009, **163**, 1310–1314.
66 Y. C. Zhang and G. L. Wang, Solvothermal synthesis of CdO hollow nanostructures from CdO_2 nanoparticles, *Mater. Lett.*, 2008, **62**, 673–675.
67 A. Zaoui and M. Ferhat, *Phys. Lett. A*, 2017, **381**(7), 685–688.
68 N. Goubet, M. Thomas, C. Greboval, A. Chu, J. Qu, P. Rastogi, S. S. Chee, M. Goyal, Y. Zhang, X. Z. Xu, G. Cabailh, S. Ithurria and E. Lhuillier, *J. Phys. Chem. C*, 2020, **124**, 8423–8430.
69 A. Bafekry, M. M. Obeid, C. V. Nguyen, M. Ghergherehchi and M. Bagheri Tagani, *J. Mater. Chem. A*, 2020, **8**, 13248–13260.
70 M. H. Hudson, M. Chen, V. Kamysbayev, E. M. Janke, X. Lan, G. Allan, C. Delerue, B. Lee, P. G. Sionnest and D. V. Talapin, *ACS Nano*, 2018, **12**, 9397–9404.
71 M. Chen, X. Lan, X. Tang, Y. Wang, M. H. Hudson, D. V. Talapin and P. Guyot-Sionnest, *ACS Photonics*, 2019, **6**, 2358–2365.
72 H. Eidsvag, M. Rasukkannu, D. Velauthapillai and P. Vajeeston, *RSC Adv.*, 2021, **11**, 3759–3769.
73 J. Xu, Sh. Lai, M. Hu, Sh. Ge, Ru. Xie, F. Li, D. Hua, H. Xu, H. Zhou, R. Wu, J. Fu, Y. Qiu, J. He, Ch. Li, H. Liu, Y. Liu, J. Sun, X. Liu and J. Luo, *Small Methods*, 2020, **4**, 2000567.
74 L. Najafi, S. Bellani, R. Oropesa-Nuñez, B. Martín-García, M. Prato, L. Pasquale, J.-K. Panda, P. Marvan, Z. Sofer and F. Bonaccorso, *ACS Catal.*, 2020, **10**, 3313–3325.
75 J. Gao, Y. Cheng, T. Tian, X. Hu, K. Zeng, G. Zhang and Y.-W. Zhang, *ACS Omega*, 2017, **2**, 8640–8648.
76 C. Cheng, J.-T. Sun, X.-R. Chen and S. Meng, *Sci. Bull.*, 2018, **63**, 85–91.
77 M. J. Mleczko, Ch. Zhang, H. R. Lee, H.-H. Kuo, B. Magyari-Kope, R. G. Moore, Z.-X. Shen, I. R. Fisher, Y. Nishi and E. Pop, *Sci. Adv.*, 2017, **3**(8), e1700481.
78 J. P. Perdew, K. Burke and M. Ernzerhof, Generalized gradient approximation made simple, *Phys. Rev. Lett.*, 1996, **77**, 3865.
79 J. P. Perdew, K. Burke and M. Ernzerhof, Generalized gradient approximation made simple, *Phys. Rev. Lett.*, 1997, **78**, 1396.
80 J. Heyd, G. E. Scuseria and M. Ernzerhof, Screened hybrid density functionals applied to solids, *J. Chem. Phys.*, 2003, **118**, 8207.
81 G. Kresse and J. Hafner, Ab initio molecular dynamics for liquid metals, *Phys. Rev. B: Condens. Matter Mater. Phys.*, 1993, **47**, 558.
82 G. Kresse and J. Hafner, Efficient iterative schemes for ab initio total-energy calculations using a plane-wave basis set, *Phys. Rev. B: Condens. Matter Mater. Phys.*, 1994, **49**, 14251.
83 R. F. W. Bader, *Atoms in molecules: a quantum theory*, Oxford University Press, 1994, p. 458, ISBN: 978-0-19-855865-1.
84 H. J. Monkhorst and J. D. Pack, Special points for Brillouin-zone integrations, *Phys. Rev. B: Solid State*, 1976, **13**, 12.
85 D. Alfe, PHON: A program to calculate phonons using the small displacement method, *Comput. Phys. Commun.*, 2009, **180**, 2622.
86 J. Tersoff and D. R. Hamann, Theory of the scanning tunneling microscope, *Phys. Rev. Lett.*, 1983, **50**(25), 1998–2001.
87 I. Horcas, R. Fernandez, J. M. Gomez-Rodriguez, J. Colchero, J. Gomez-Herrero and A. M. Baro, *Rev. Sci. Instrum.*, 2007, **78**(1), 013705.